ZIBELINE INTERNATIONAL™ PUBLISHING

ISSN: 2523-5664 (Print)
ISSN: 2523-5672 (Online)
CODEN: WCMABD

Water Conservation & Management (WCM)

DOI: http://doi.org/10.26480/wcm.01.2022.61.69

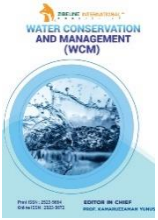

RESEARCH ARTICLE

EVALUATION OF ERA5 AND IMERG PRECIPITATION DATA FOR RISK ASSESSMENT OF WATER CYCLE VARIABLES OF A LARGE RIVER BASIN IN SOUTH ASIA USING SATELLITE DATA AND ARCHIMEDEAN COPULAS

Surajit Deb Barma[a]*, Sameer Balaji Uttarwar [b], Prathamesh Barane[a], Nagaraj Bhat[c], Amai Mahesha[a]

[a] Department of Water Resources and Ocean Engineering, National Institute of Technology Karnataka, Surathkal, Mangaluru – 575025, India.
[b] Department of Civil, Environmental and Mechanical Engineering, University of Trento, Via Mesiano, 77, 38123 Trento TN, Italy.
[c] Department of Computer Science and Engineering, SMVITM, Bantakal, Udupi - 574 115, India.
**Corresponding Author Email: surajitdb@gmail.com*

ARTICLE DETAILS

Article History:

Received 15 September 2021
Accepted 14 January 2022
Available online 28 February 2022

ABSTRACT

Precipitation as a major water cycle variable influences the occurrences and distribution of terrestrial water storage change (TWSC), evapotranspiration (ET), and river discharge (Q) of a large river basin. However, its relationship with the other water cycle variables using probabilistic dependence structure concept has not been addressed much. Furthermore, precipitation derived from gauge record is plagued by bias due to orography and under-catch. To fill these gaps, bivariate copula and precipitation derived from reanalysis and satellite data were used. In the present study, the basin-wide averages of the precipitation products APHRODITE, ERA5, and IMERG were used as predictors, whereas the areal mean of MOD16 evapotranspiration, GRACE TWSC, and gauge discharge were used as dependent variables (predictants) for the Brahmaputra basin. The bivariate Archimedean copulas were applied to all the pairs of precipitation-TWSC, precipitation-ET and precipitation-Q based on the optimal marginal distributions obtained. Using the best copula for each pair of the variables, the conditional probability was constructed to predict the predictants for different precipitation amounts (5th, 25th, 50th, 75th, and 95th percentiles). The focus of the analysis was on two scenarios of the predictants (i.e.,≤ 5th and ≥ 95th percentiles). The non-exceedance conditional distribution of TWSC, ET, and Q (all predictants ≤ 5th percentile) decreases with precipitation increase. However, the exceedance probability of the predictants (≥ 95th percentile) increases gradually with an increase in precipitation. The results revealed that both ERA5 and IMERG precipitation data could be used to derive probabilistic measures of the water cycle variables in the absence of gauge-based precipitation.

KEYWORDS

APHRODITE, GRACE TWSC, MOD16 ET, discharge, Brahmaputra

1. INTRODUCTION

The relationship between precipitation and hydrologic variables is critical in understanding the occurrence of such variables in a hydrologic system. In order to attain water security and improved flexibility to hydrologic extrema, a pragmatic discernment of water resources evolution at the basin level is necessary (Sheffield et al., 2018). This is evident when dealing with the water budget of large river basins. The Pearson's correlation coefficient has been widely used in hydrology to relate one variable with another, but this statistical metric follows the assumption that the data follows normal distribution and are linear. Moreover, correlation coefficient is very sensitive to outliers (Legates and McCabe, 1999).

However, hydrometeorological variables are often known to be non-linear and rank-based correlation coefficients like Spearman's rho and Kendal's tau are preferred (Li et al., 2015; Uttarwar et al., 2020). Accordingly, prediction of a hydrological variable is carried out using various methods, namely, ordinary least square (OLS), multiple linear regression (MLR), partial least squares regression (PLSR), principal component analysis/regression (PCA/PCR) and geographically weighted regression (GWR), empirical method- Budyko framework (Li and Quiring, 2021), machine learning algorithms, conceptual hydrological model (Poncelet et al., 2017) and semi-distributed/ distributed models (Hasan and Tarhule, 2020; Jato-Espino et al., 2017; Ndehedehe et al., 2016; Sinha et al., 2019; Abudu et al., 2010; Hu et al., 2021; Yuan et al., 2019; Zhou et al., 2020; Abudu et al., 2010; Almanaseer and Sankarasubramanian, 2012; Li et al., 2020; Li and Quiring, 2021; Han et al., 2021; Seyoum and Kwon, 2020; Sinha et al., 2019; Sun et al., 2014; Sahana and Timbadiya, 2020; Sridhar et al., 2019).

For example, researchers investigated the long-term terrestrial water storage anomaly from GRACE data as affected by precipitation, runoff, surface water storage, soil moisture storage and population density using geographically multiple regression (GMR), ordinary least square (OLS) and geographically weighted regression (GWR) (Hasan and Tarhule, 2020). It is reported that GWR is important for accounting the spatial locations to characterize the variability of GRACE TWSA long-term trends in space. In the assessment of watershed characteristics on long term water balances, machine learning algorithms like neural network (ANN)

Quick Response Code	Access this article online	
	Website: www.watconman.org	**DOI:** 10.26480/wcm.01.2022.61.69

Cite the Article: Surajit Deb Barma, Sameer Balaji Uttarwar, Prathamesh Barane, Nagaraj Bhat, Amai Mahesha (2022). Evaluation of ERA5 and IMERG Precipitation Data for Risk Assessment of Water Cycle Variables of a Large River Basin in South Asia Using Satellite Data and Archimedean Copulas. *Water Conservation & Management, 6(1): 61-69.*

and relevance vector machine (RVM) were found to perform better than MLR in determining the watershed parameter (Sinha et al., 2019). PLSR and global hydrological models were used to predict terrestrial water storage (TWS) over central Asia using multiple satellite data (Hu et al., 2021). PLSR was found to be useful for simulation of the hydroclimatic variables and prediction of TWS.

A group of researchers used large sample hydrological approach and conceptual lumped hydrological model to estimate runoff variations over different landscape spread over Austria, France and Germany (Poncelet et al., 2017). The consistency of four precipitation products and GRACE TWS over the Arabian Peninsula was assessed using multivariate statistical approach and Pearson's correlation coefficient (Wehbe et al., 2018). In another study, satellite-based precipitations TRMM and CHIRPS were assessed against gauge-based precipitation to evaluate their performance in reproducing streamflow and hydrological signatures of a humid tropical catchment in India (Sharannya et al., 2020). However, limited studies have focused on the probabilistic dependence of precipitation and other water cycle variables using copula.

In order to obtain the probabilistic prediction, the dependence structure between the water cycle variables needs to be achieved using copulas. Copulas are multivariate techniques used to derive the dependence structure between two or more continuous/discrete variables (Genest and Favre, 2007; Nelsen, 2006). Copulas have been extensively applied in various fields. For example, in the area of hydrologic sciences, copulas find applications in the dependence of hydroclimatic variables, drought characterization, flood frequency analysis, compound climate extreme events, variance-based sensitivity analysis, among others (Uttarwar et al., 2020; Sajeev et al., 2021; Muthuvel and Mahesha, 2021; Hao et al., 2018; Tavakol et al., 2020; Zscheischler and Seneviratne, 2017; Sheikholeslami et al., 2021).

Copulas have also been increasingly applied to make a probabilistic prediction of a dependent variable using conditional distribution concepts. Ahn and Palmer explored nonstationary frequency analysis of annual low flow in the Connecticut River Basin, United States using nonstationary and stationary copula approaches (Ahn and Palmer, 2016). Due to the outcome of nonstationary copulas, their findings show the existence and intensity of low flows to be lesser for the same probability. Given the dependence structure of precipitation-streamflow, a group of researchers estimated the conditional distribution of required environmental flow for different precipitation scenarios for three watersheds of varying sizes from China, Germany, and the USA (Liu et al., 2016). Their results show that the joint streamflow drought index could help indicate the wetness/dryness for drought onset determination and persistence.

Similarly, the meta-Gaussian model was used to predict standardized runoff index (SRI) given the standardized precipitation index (SPI) in the conditional distribution framework for ten climate divisions in Texas, USA (Hao et al., 2016). A group of researchers applied the concept of the conditional marginal distribution of suspended sediment load (SSL) given discharge level for seven significant rivers in the USA (Shojaeezadeh et al., 2018). In another similar study, the infilling of suspended sediment load was carried out using conditional distribution of suspended sediment load given discharge in Jenshou station, Hualian River of eastern Taiwan (Shiau and Lien, 2021). Liu and Menzel investigated the probabilistic dependence structure between river discharge and climatic variables and the associations to large atmospheric oscillation over Baden-Württemberg in Southwest Germany (Liu and Menzel, 2018). A group of researchers applied bivariate copula model to derive combined distributions of air-water temperatures and streamflow-water temperature and subsequently used conditional probability distribution to predict maintainable water temperature for maintaining the ecology in the river given air temperature and discharge for the central extent of the Yangtze River in China (Tao et al., 2020).

Precipitation is often the most significant component of the water cycle. The main caveat with gauge-based precipitation is wind-induced under catch and the altitude bias gauge deployment apart from many other quantification impediments (McCabe et al., 2017). It is also sparsely recorded in mountainous regions with varying topographic features. Reanalysis data are obtained from model runs and are not gauge corrected. Satellite-based precipitation has better spatial coverage than gauge-based precipitation, but it can under/over predict low/high precipitation depending on the climate of a region. Hence, gauge, reanalysis, and satellite-based precipitation products were used as independent variables in this study. TWSC, ET, and Q were used as dependent variables using dependence structure in copula for the Brahmaputra basin as a case study.

Moreover, to the best of the authors' knowledge, no such study was conducted for a large river basin like the Brahmaputra on the dependence measure between precipitation from Asian Precipitation Highly Resolved Observational Data Integration Towards Evaluation of the Extreme Events (APHRODITE), ERA5 reanalysis, and Integrated Multi-satellitE Retrievals for GPM (IMERG), and TWSC, ET, and Q. This study could be extended for any large river basin worldwide. The principal goal of the current research is to make probabilistic predictions of TWSC, ET, and Q for different precipitation scenarios. We hypothesize that precipitation is a good predictor of the dependent water budget variables. Accordingly, the following research questions were attempted: (1) Which optimal marginal distribution describes each water cycle variable? (2) Which is the optimal copula for a given pair of precipitation-TWSC, precipitation-ET, and precipitation-Q? (3) How well can each precipitation product help to predict TWSC, ET, and Q?

2. MATERIALS AND METHODS

2.1 Case Study area

The Brahmaputra basin lies between 25°–32° North latitude and 82°–98°East longitude. The basin with an average discharge of about 20,000 m^3s^{-1} is the fourth largest river in terms of the quantity of runoff in the world (Jian et al., 2009). The total drainage basin area is about 517,224 km^2 at Bahadurabad gauging station. Bhutan and Bangladesh share about 8% each, about 34% in India, and about 50% in China (Figure 1) (Immerzeel, 2008). The Brahmaputra's source originates from the Chemayungdung Glacier and throughout the upper part in Tibet, it is known by Tsangpo (purifier in Tibet) and in Chinese "Yarlung Zangbo" (Ahmad and Lodrick, 2017). In contrast, the lower part of the river in India and Bangladesh is known as Brahmaputra ("son of Brahma"). From the origin, it flows for about 1150 km eastwards. Then it enters the northern-most point of Arunachal Pradesh (India), turns southwards, and flows for nearly 500 km, it directs towards west-flowing through the states of Arunachal Pradesh, Assam, and Meghalaya for next about 700 km before it finally moves into Bangladesh (Futter et al., 2015). The Tibetan Plateau bifurcates the basin into two unique zones of climate: (1) the northern part of the basin is dominated by mountain climate and is characterized as cold and dry; and (2) the southern part is dominated by the tropical monsoon climate and is categorized as humid and warm thereby receiving high amount of precipitation under the impact of the Indian summer monsoon (Pervez and Henebry, 2015). The Brahmaputra is characterized by braided channels, whereas the Ganges meandering channels (Futter et al., 2015). It is topographically and ecologically abundant in crops and natural biodiversity falling into three distinct topographic areas: (a) the Tibetan Plateau covering 44% of the area with 3500 m and above high, (b) the Himalayan section covering 29% with 100 – 3500 m and (c) the floodplains covering 27% with below 100 m elevation (Immerzeel, 2008). The river is a lifeline to nearly 70 million people who depend on water resources for food production (Hasson et al., 2013).

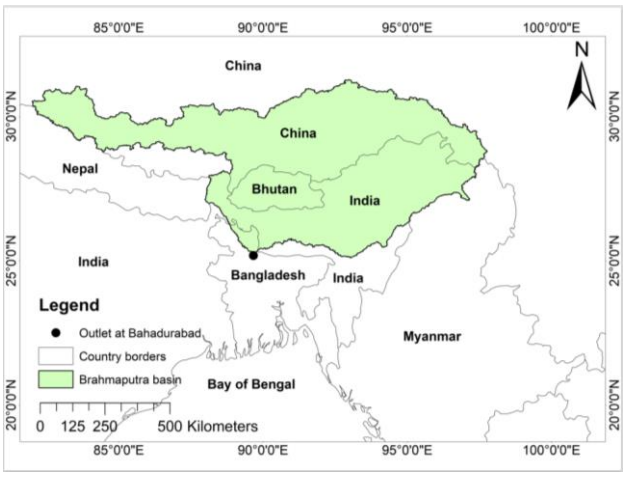

Figure 1: Study area map of Brahmaputra basin

2.2 Data sets

The first step toward water budget analysis is obtaining precipitation data, often sparse for poorly gauged basins like the Brahmaputra. Precipitation is also the most widely used independent variable in hydrological investigations. To assess the utility of precipitation data derived from various sources, viz., gauge-based, reanalysis, and gauge-corrected satellite and satellite data, monthly probabilistic assessments of terrestrial

water storage change (TWSC), evapotranspiration (ET), and streamflow were carried out.

2.2.1 Precipitation

2.2.1.1 APHRODITE gauge data

The Asian Precipitation Highly Resolved Observational Data Integration Towards Evaluation of the Extreme Events (APHRODITE) V1101 is available on a daily scale for the year 1951-2007 at 0.25/0.50 degrees spatially, but APHRODITE-2 (V1901) is available from 1998 to 2015 for the exact spatiotemporal resolution for whole of Asia (Yatagai et al., 2012). The main improvement of V1901 is the 24-hour accumulation period adjustment to the 00 - 24 UTC of the stamped date. The other improvement in APHRODITE-2 (V1801 and V1901) was the daily climatology used as a ratio of daily rainfall to the climatology to interpolate the gauge data. In contrast, monthly climatology was used for older versions. The long-term version has been applied in various studies and found to be performing well. However, the newer version is yet to be evaluated on a large scale though it was found to perform well with respect to gauge data in the Brahmaputra basin (Ji et al., 2020). In V1801 and V1901, the end of the day (EOD) was matched using the satellite-based precipitation CMORPH, and the extreme values were identified using CMOPRH and TRMM-3B42. The monthly areal average precipitation for the Brahmaputra basin was derived from daily data from 2003 to 2014 for the current study from http://aphrodite.st.hirosaki-u.ac.jp/download/.

2.2.1.2 ERA5 reanalysis data

The ERA5 is the 5th reanalysis product and replacement to ERA-Interim and all previous versions of the European Centre for Medium-Range Weather and Forecasting (ECMWF) reanalysis (Hersbach et al., 2020). In a comparative study to ERA-Interim and Global Precipitation Climatology Project (GPCP) as the base data for the 1979–2018 period, Nogueira found that ERA5 showed lower bias as well unbias root-mean-squared error and higher correlations over most of the tropics and limited regions of mid-latitudes (Nogueira, 2020). However, ERA-Interim outperformed ERA5 over the Himalayas. Overall, ERA5 has improved parameterization and better resolution leading to trade-off performances over most of the regions. The monthly areal mean ERA5 precipitation (0.25-degree lat/long) data was downloaded from the Google Earth Engine platform for 2003 to 2014.

Before using any precipitation product, it is recommended that the product be assessed against the gauge-based product in terms of the three categorical metrics: POD (1), FAR (0), and CSI (1), and the continuous metrics, viz., r (0), RBIAS (0), ME (0), MAE (0), and RMSE (1). The numerical figures within the braces are the optimal values of the corresponding metric. For more details, the work of the categorical metrics and the continuous metrics may be referred from literature (AghaKouchak and Mehran, 2013; Duan et al., 2016). Since the focus of the current study is at the basin level, no pixel-to-pixel and grid-to-grid level assessments were carried out. The daily and monthly performance metrics were tabulated in Table 1. The diurnal POD is 0.88, which is the fraction of ERA5 correctly representing the actual occurrence of precipitation against APHRODITE. The monthly POD is 1 as expected because precipitation at this scale results from the daily precipitation that occurs on either of the days of a month.

Table 1: Performance metrics of ERA5 and IMERG against APHRODITE

Statistical Metric	ERA5		IMERG	
	Daily	Monthly	Daily	Monthly
Probability of detection (POD)	0.88	1	1	1
False alarm ratio (FAR)	0.01	0	0.03	0
Critical success index (CSI)	0.87	1	0.97	1
Pearson's correlation coefficient (r)	0.91	0.99	0.91	0.99
Relative bias (RBIAS)	0.95	0.95	0.25	0.25
Mean error (ME)	2.77	84.37	0.73	22.44
Mean absolute error (MAE)	0	0.19	0	0.01
Root mean squared error (RMSE)	4.07	100.09	2.27	32.79

The daily FAR is of negligible magnitude of 0.01, which is the proportion of precipitation detected by ERA5 but not confirmed by APHRODITE. The monthly FAR is 0, which is likely to occur because a single day of rain in a given month is enough for FAR to be of this magnitude for that month when it has actually not occurred. The daily and monthly CSI are respectively 0.87 and 1. This metric is the combination of POD and FAR and is also known as threat score representing the overall score of ERA5 against APHRODITE. The daily correlation coefficient between ERA5 and APHRODITE is 0.91, which indicates good linear strength. The monthly correlation increases slightly to 0.99. The daily and monthly BIAS is 0.95, which means ERA5 is outperforming against APHRODITE. The daily ME, MAE, and RMSE are 2.77, 0, and 4.07 mm, respectively, whereas the monthly ME, MAE, and RMSE are 84.37, 0.19, and 100 mm, respectively. All the monthly categorical and continuous statistics are higher than the daily ones (except for BIAS) but at the cost of having higher error metrics primarily due to temporal resolution effects.

2.2.1.3 GPM IMERG satellite-based data

The final run (FR) global precipitation measurement (GPM) resulted in the program known as the Integrated Multi-satellitE Retrievals for GPM (IMERG). The rainfall was derived from several satellite passive microwave (PMW) sensors encompassing the GPM collection using the Goddard Profiling Algorithm of 2017(GPROF2017) (Huffman et al., 2019). The inter-calibration of the gridded data (0.1°x0.1°; June 2000 onwards) to the Combined Ku Radar-Radiometer Algorithm (CORRA) of GPM product on 30-minute basis with adjustment to Global Precipitation Climatology Project (GPCP) in-situ satellite product was carried out to rectify identified errors over high-latitude ocean and tropical land. Though the precipitation product comes in half-hourly, daily, and monthly scales, the latter two were derived from the former. In this study, the monthly IMERG V06 data was obtained by summing the daily precipitation from https://disc.gsfc.nasa.gov/datasets/GPM_3IMERGDF_06/summary?keywords=GPM. A group of researchers conducted a comparative study of two products (ER=early run and FR) of IMERG for two decades over the whole globe (Li et al., 2021). ER estimated 12% more annual rainfall than FR over the land and 33% greater extreme precipitation over the earth. Since the FR is gauge-adjusted, it is used for long-term hydrometeorological studies, whereas ER is useful for short-term real-time studies like floods. The daily and monthly performance metrics of IMERG are better than ERA5 except for the correlation coefficient (r), which is the same at both the temporal scales, as shown in Table 1. Also, FAR is slightly higher but of negligible value. The performance metrics of IMERG are better than that of ERA5 as expected because IMERG is gauge-corrected, making it closer to APHRODITE.

2.2.2 GRACE Terrestrial Water Storage Change (TWSC)

The monthly variations of the earth's gravity field obtained by determining the length between two orbiting satellites since April 1st 2002 have been provided by the Gravity Recovery and Climate Experiment (GRACE) satellites (Tapley et al., 2004). For regions of 200,000 km^2 or more, GRACE data provide unprecedented accessibility to terrestrial water storage changes (with a precision of 1.5 cm equivalent water height) with respect to climate change, global change, human water use, groundwater extraction, which is unmeasured and unmanaged in several parts of the world. The GRACE data may be freely accessed from three different sources: the Jet Propulsion Laboratory (JPL), the Center for Space Research (CSR) at the University of Texas, and Geoforschungs Zentrum Potsdam (GFZ). These three products were obtained following the spherical decomposition of GRACE records. It is usually recommended to use the average of the three products to reduce uncertainty. Another category of GRACE records is the MASCON (mass concentration) dataset, which comes independently from JPL and CSR (Watkins et al., 2015). The solution from JPL is explicit, whereas the one from CSR is first spherically decomposed. In the current study, the solution from JPL is used because it is independent (Pellet et al., 2020). In this study, a simple derivative method representing the total water storage change ($TWSC$) between two data points in terms of mass anomalies is used and may be presented as (Oliveira et al., 2015; Wang et al., 2014):

$$\frac{ds}{dt} = \frac{TWSA}{dt} = \frac{TWSA(t+1) - TWSA(t)}{\Delta t} \quad (1)$$

where S is the change in water storage with respect to time t, $TWSA$ is terrestrial water storage anomaly. The basin-average of GRACE data was used for the current analysis.

2.2.3 MOD16 Evapotranspiration (ET)

The evapotranspiration forms a significant part of the water cycle that

influences irrigation planning and crop water requirement. This study uses the MOD16 ET product, the derivative of GMAO (Global Meteorological Assimilation Office) climate, and MODIS global terrestrial evapotranspiration dataset obtained via Penman-Monteith equation (Mu et al., 2011). The cumulative evapotranspiration includes day and night components with soil heat flux calculation and improvement estimates of stomatal conductance from damp topsoil and covering surfaces of plants. MOD16 is also one of the most widely used ET products. A monthly product at a spatiotemporal resolution of 0.05 degree from the 1st month of 2003 to the last month of 2014 was used for the study after downloading from http://files.ntsg.umt.edu/data/NTSG_Products/MOD16/. The dataset was spatially averaged over the Brahmaputra basin for further analysis.

2.2.4 Discharge Data

The daily water level (5 times a day) and weekly discharge (using the velocity-area method) of the Brahmaputra basin at Bahadurabad station are recorded by the Hydrology Division belonging to the Bangladesh Water Development Board (BWDB) (Masood et al., 2015). The daily water level and weekly discharge were used to construct rating curves (personal communication) to calculate the daily discharge. The daily discharge for 2003-2014 was converted to monthly values by averaging the daily discharge in cumecs (m^3/s).

2.3 Methods

The dependence measure between random variables is often determined using Pearson's correlation based on the normal distribution. However, such an assumption could be misleading while dealing with hydrometeorological variables having a nonlinear relationship between such random variables. Moreover, a nonlinear relationship also warrants the application of non-normal distributions. In this context, copula has been around for nearly two decades in hydrologic sciences opening up new understanding and insights embedded in hydrometeorological variables. The copula is attractive and advantageous over traditional bivariate methods. It is flexible to model two random variables (bivariate case) irrespective of the marginal distributions and handle linear and nonlinear variables. According to Sklar's theorem, if X and Y are the continuous random variables, then their joint distribution $H_{XY}(x, y)$ and $C: [0,1]^2 \rightarrow [0,1]$ copula are connected as (Sklar's, 1959):

$$H_{XY}(x, y) = F_{XY}(x, y) = C[F_X(x), F_Y(y)] = C(u, v), x, y \in R \quad (2)$$

where $F_X(x)$ and $F_Y(y)$ are the cumulative distribution functions of X and Y, respectively. In general, Archimedean copulas carry the following expressions:

$$C(u, v) = \phi^{[-1]}[\phi(u) + \phi(v)],\ u, v \in [0,1] \quad (3)$$

where $\emptyset(\bullet)$ is a generator function of the copula and $\emptyset^{[-1]}(\bullet)$ is the pseudo-inverse of $\emptyset(\bullet)$. The flexibility and ease of construction make Archimedean copulas widely used in different research areas with well-established copula functions (Genest and Favre, 2007; Nelsen, 2006; Zhang and Singh, 2006). The Archimedean copulas, viz., Clayton, Frank, and Gumbel-Hougaard copulas, were applied in this study. The details of such copulas are found in (Wable and Jha, 2018). The conditional distribution of a continuous variable for a value of another continuous variable could be obtained once the joint probability distribution function between the random variables is known. Then for the bivariate case, the probability distribution of U conditioned on $V \leq v$ is given by (Uttarwar et al., 2020; Zhang and Singh, 2006):

$$C_{(U|V \leq v)} = C(U \leq u | V \leq v) = \frac{C(u, v)}{v} \quad (4)$$

In the present study, the single-parameter copulas were used to study the two extrema of TWSC, ET, and streamflow, viz., non-exceedance probability ($\leq$ 5th percentile) for the lower extreme and the exceedance probability ($\geq$ 95th percentile) for the upper extreme given different scenarios of precipitation (5th, 25th, 50th, 75th, and 95th percentiles).

The following steps were followed for the current study:

(i) Select any two random variables between a precipitation dataset and TWSC or ET or streamflow.

(ii) Determine the significant dependence measure using Spearman's rho for the two selected variables, for example, precipitation and TWSC. The correlation will help us decide whether to go ahead with dependence modeling.

(iii) Fit the parametric theoretical distributions, viz., gamma, logistic, lognormal, and Weibull to precipitation, TWSC, ET, and streamflow. The best fit marginal distribution for each variable is obtained using the Kolmogorov–Smirnov (KS) goodness of fit test.

(iv) Obtain copula parameter using the pseudo-maximum-log-likelihood method (1000 simulations) for all the copulas.

(v) Obtain the best fit copula based on Akaike Information Criterion (AIC), the lowest being the best.

(vi) Derive conditional probability distribution of TWSC, ET, and streamflow given the explanatory variable, precipitation.

3. Results

3.1 Identification of Marginal Distribution of Precipitation, TWSC, ET, and Discharge

The best marginal distribution for APHRODITE and IMERG precipitation is gamma at 5% significance level and lognormal for ERA5 precipitation at 10% significance level as per the KS statistics shown in Table 2. The optimal marginal distribution for ERA5 and the other two precipitations could be due to differences in magnitudes; especially lower values of ERA5 are higher than those of the other two precipitation products. Moreover, IMERG is gauge-corrected satellite precipitation, which could resemble APHRODITE derived from gauge precipitation.

Table 2: KS statistics of different marginal distributions fitted to precipitation

Marginal Distribution	APHRODITE	ERA5	IMERG
Gamma	**0.1112** (0.0539*)	0.0769 (0.3483)	**0.1120** (0.0506*)
Normal/Lognormal	0.1428 (0.0056) Normal	**0.1021** (0.0945**), Lognormal	0.1515 (0.002654), Normal
Weibull	0.1128 (0.0483)	0.0771 (0.3453)	0.1143 (0.0440)

Note: * indicates 5% level of significance **indicates 10% level of significance. Bold figures indicate optimal distribution.

The theoretical cumulative distribution curves are compared with the empirical distribution for each precipitation in Figure 2. TWSC being in anomaly form could be fitted only by kernel density functions like normal and quadratic, but only normal kernel density function was fitted in this study. Hence, no KS statistics was calculated, as shown in Table 3. Logistic and lognormal distributions, respectively, best represented ET and discharge. The cumulative distribution function curves of TWSC, ET, and discharge are presented in Figure 3 compared to their corresponding empirical distribution curves.

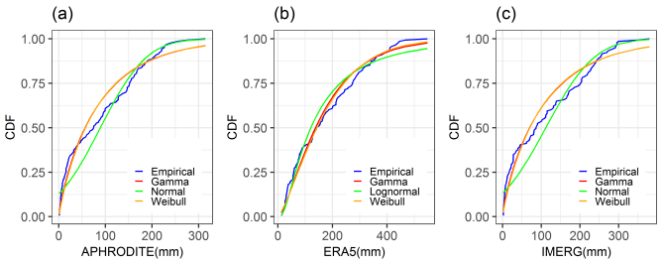

Figure 2: Cumulative distribution function plots of precipitation products

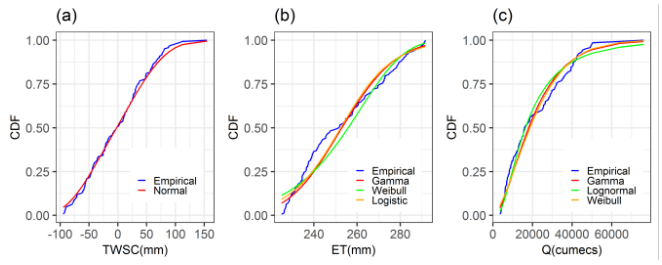

Figure 3: Cumulative distribution function plots of dependent variables

3.2 Dependence Modeling of Precipitation with TWSC, ET, and Discharge

The bivariate Archimedean copulas were constructed using the optimal marginal distribution for each variable. Though all the Archimedean copulas were simulated, only the optimal copulas based on AIC measures (27 AIC values of that many pairs are not shown here for the sake of brevity) are shown in Table 4. Then, Pearson's linear and Spearman's rank correlations were obtained for each pair of variables (Tao et al., 2020). All the pairs are either optimally represented by Frank or Clayton copulas, as shown in Table 4. The correlations (Pearson's and Spearman's) between all precipitation products (APHRODITE, ERA5, and IMERG) and TWSC and ET are significant for both observed and simulated data.

Table 3: KS statistics of different marginal distributions fitted to dependent variables

Marginal Distribution	TWSC	Evapotranspiration (ET)	Discharge (Q)
Gamma	-	0.1169 (0.0369)	0.0842 (0.2483)
Weibull	-	0.1282 (0.0165)	0.0832 (0.2607)
Logistic/ Lognormal	-	**0.1059** (0.0751**), logistic	**0.1095** (0.0599*)
Normal kernel	Optimal	-	-

Note: * indicates 5% level of significance **indicates 10 % level of significance. Bold figures indicate optimal distribution

Table 4: Performance measures of the optimal copula of different pairs of the water cycle variables

Pair	Optimal Copula	Copula Parameter (Θ)	Pearson's Linear Correlation (r)		Spearman's Rank Correlation (ρ)	
			Observed	Simulated*	Observed	Simulated*
APHRODITE_TWSC	Frank	5.9233	0.7639	0.5911	0.7658	0.7083
ERA5_TWSC	Frank	6.3882	0.7786	0.5553	0.7733	0.7511
IMERG_TWSC	Frank	5.5380	0.7437	0.6041	0.7517	0.7240
APHRODITE_ET	Clayton	2.1978	0.9024	0.4989	0.8893	0.7007
ERA5_ET	Frank	9.2382	0.8895	0.6182	0.8718	0.8371
IMERG_ET	Clayton	2.3581	0.9107	0.5499	0.8956	0.7491
APHRODITE_Q	Clayton	0.2606	0.4237	0.0903	0.3829	0.1863
ERA5_Q	Frank	1.6343	0.3871	0.2239	0.3514	0.5971
IMERG_Q	Clayton	0.2888	0.4531	0.1032	0.4008	0.1905

Note: *Correlation is calculated from simulation values of 1000 data samples.

However, the correlations of the precipitation products with discharge are significant only for the observed values. In comparison, the correlations for simulated precipitation-discharge pairs are lesser. The correlations for precipitation-TWSC and precipitation-ET pairs are higher than those of precipitation-discharge pairs because the lags between the pairs may not influence much on the dependence measure of the first two pairs than the last pair. This is true when precipitation occurs; ET also occurs without much time lag. The same is true with the occurrence of precipitation; the amount of TWSC is manifested with little elapse of time. The commonly rainfall-runoff concept demonstrates how rainfall occurring at a particular time in a given day or cumulative rainfall occurring in a given month may influence discharge at the outlet in days or months. As a result, the dependence measure expressed in Spearman's rank correlation and Pearson's linear correlation is found to be lesser for the precipitation-discharge pair than the other two pairs.

The scatter diagrams in Figure 4 and Figure 5 show that the simulated values of precipitation-TWSC and precipitation-ET pairs represent the observed values well. The scatter plots of APHRODITE and IMERG with TWSC look similar in pattern because both precipitations are connected to the gauge dataset. The scatter plots (Figure 6) for precipitation-discharge look different from the other two pairs, as evident from the linear and rank correlations.

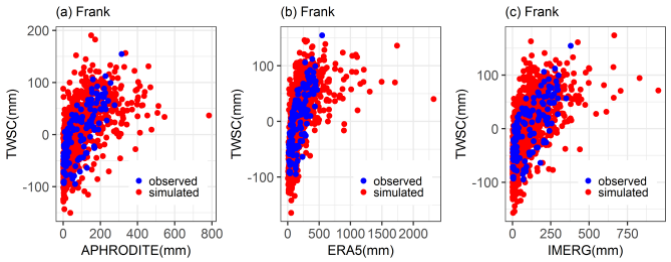

Figure 4: Scatter diagrams of different precipitation-TWSC pairs

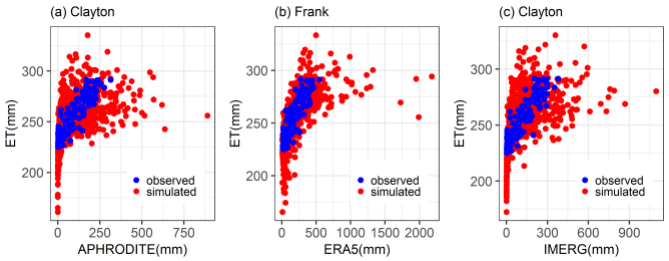

Figure 5: Scatter diagrams of different precipitation-ET pairs

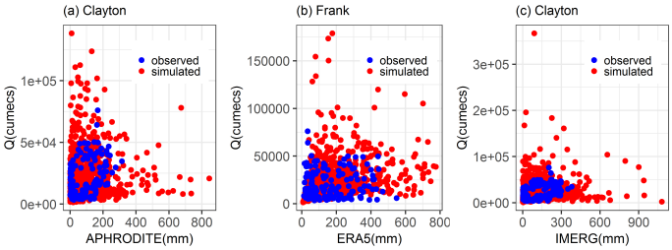

Figure 6: Scatter diagrams of different precipitation-Q pairs

3.3 Risk Evaluation of TWSC Conditioned on Different Precipitation Scenarios

The conditional distribution of TWSC under different precipitation scenarios could be evaluated once the joint distribution between TWSC and a given precipitation scenario is obtained. The risk evaluation of the occurrence of an event is associated with the exceedance/ non-exceedance of the TWSC for a given threshold of explanatory variable precipitation (Liu et al., 2018; Salvadori and De Michele, 2004). The next step is to evaluate the probability of occurrence of TWSC under five different precipitation scenarios on establishing joint distribution, as shown in Table 4. In order to achieve this, two scenarios of TWSC were investigated

(TWSC ≤ 5th percentile and TWSC ≥ 95th percentile as shown in Table 6) for every precipitation scenario. For example, the probabilities of occurrence of an event (TWSC ≤5th percentile from Figure 7) for different scenarios of gauge-based APHRODITE precipitation are 28%, 26%, 16%, 10%, and 8%, corresponding to 5th, 25th, 50th, 75th, and 95th percentiles, respectively.

Table 5: Magnitudes of precipitation corresponding to each percentile

Precipitation	Percentile				
	5th	25th	50th	75th	95th
APHRODITE (mm)	2.7453	15.2911	74.5768	151.8014	205.0797
ERA5 (mm)	24.2	58.5	144	274	361.6
IMERG (mm)	3.177638	17.78558	86.51642	201.9606	253.9442

Table 6: Magnitudes of the dependent variable corresponding to each percentile

Dependent Variable	Percentile	
	5th	95th
TWSC (mm)	-84.1232	71.7037
Evapotranspiration (ET) (mm)	227.0304	281.7144
Discharge(Q) (m^3/s)	4751.536	42238.01

Similarly, the probability of the lower value of TWSC (≤5th percentile) for the same scenarios of precipitation of gauge-corrected satellite-based GPM-IMERG and reanalysis ERA5 follows a very similar pattern. The conditional distribution of TWSC ≥ 95th percentile (Figure 7) increases with precipitation (for the same precipitation scenarios). For example, the conditional distribution of TWSC for APHRODITE precipitation scenarios is less than 1% for 5th (100 – 99.718 = 0.28%), 25th (0.32%), and 50th (0.83%) percentiles. However, the conditional probabilities are about 4% and 8%, respectively, for precipitation less than equal to 75th and 95th percentiles. Similar is the case for GPM-IMERG and ERA5.

3.4 Risk Evaluation of ET Conditioned on Different Precipitation Scenarios

The joint distribution of APHRODITE-ET is applied to obtain the conditional distribution of ET for different scenarios of APHRODITE. The conditional probabilities of ET ≤ 5th percentile (Table 6) (Figure 8(a)) are 92, 48, 18, 13, and 12 %, corresponding to the APHRODITE precipitation values at 5th, 25th, 50th, 75th, and 95th percentiles.

Similarly, the conditional probabilities of ET at its lower end (≤ 5th percentile) given the precipitation scenarios of IMERG are almost identical to that of APHRODITE. However, the conditional probabilities of ET given the scenarios of ERA5 are lesser than that with the other two precipitation datasets up to ≤ 25th percentile (Figure 8(b)).

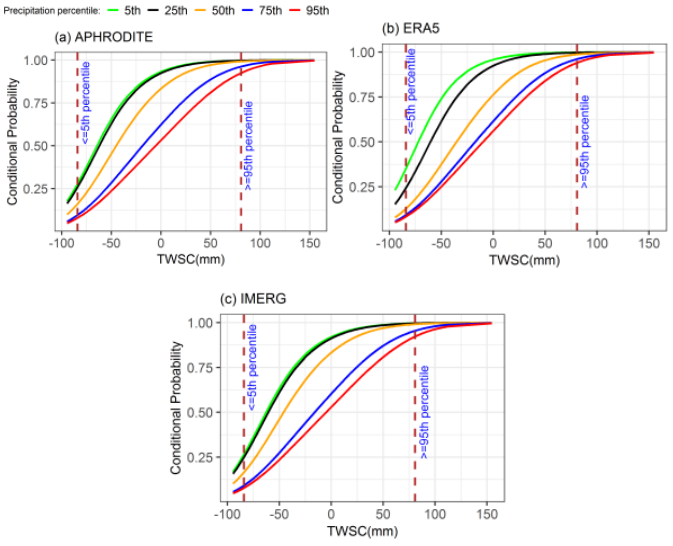

Figure 7: Conditional distribution plots of TWSC given different precipitation products

The conditional probability of mean ET (≥ 95th percentile) (Table 6) (Figure 8) for all the scenarios of precipitation lies between 0 and 5. It means that the higher events of precipitation have a lesser effect on the evapotranspiration process.

3.5 Risk Evaluation of Q Conditioned on Different Precipitation Scenarios

The conditional distributions of Q for different precipitation scenarios (5th to 95th percentiles) decrease with the increase in precipitation. The probability of the Q≤5th percentile (Table 6 and Figure 9 (a)) are approximately 20%, 12%, 7%, 6% and 6 %, corresponding to APHRODITE precipitation at 5th to 95th percentiles, respectively.

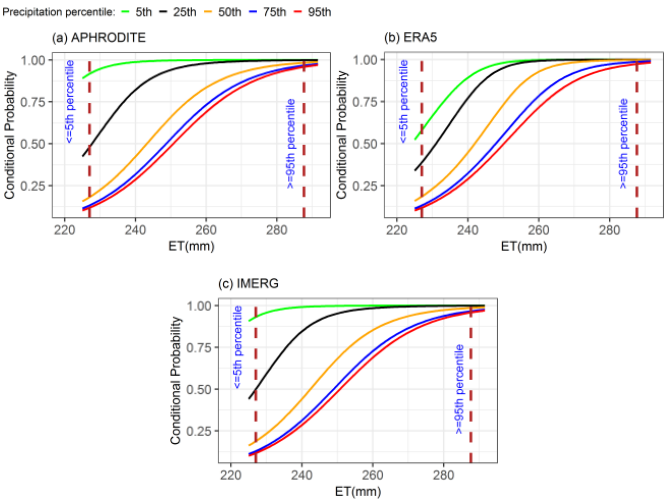

Figure 8: Conditional distribution plots of ET given different precipitation products

Similarly, the probabilities of occurrence of Q ≤5th percentile are approximately 22%, 13%, 8%, 6%, and 6 %, corresponding to IMERG precipitation (Figure 9(c)) at 5th to 95th percentiles, respectively. Furthermore, the probabilities of occurrence of Q≤5th percentile are approximately 10%, 9%, 7%, 6%, and 6 %, corresponding to ERA5 precipitation (Figure 9(b)) at 5th to 95th percentiles, respectively.

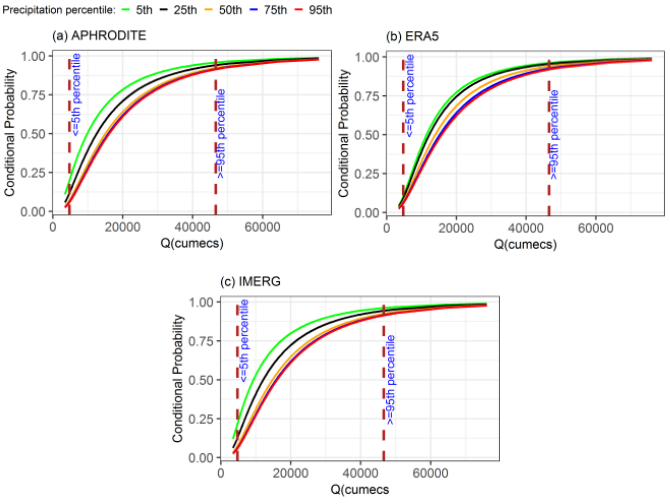

Figure 9: Conditional distribution plots of Q given different precipitation products

The conditional probabilities of the Q≥ 95th percentile (Table 6) (Figure 9) for different scenarios of precipitation increase with the increase in precipitation. Also, the probability of occurrence given the scenarios of all three precipitation products lies between 4 and 9%.

4. Discussion

The risk assessment of the occurrence of an event is the exceedance/ non-exceedance probability of the GRACE terrestrial water storage change (TWSC), evapotranspiration (MODIS-16 ET), and discharge (Q) for a given threshold of explanatory variable precipitation derived from in-situ measurement (APHRODITE), model-based reanalysis (ERA5), and gauge corrected satellite-based data (GPM IMERG). The study attempted to

probabilistically predict the dependent water budget variables, namely, TWSC, ET, and Q for five scenarios of precipitation derived from various sources. We proved the hypothesis that precipitation data ERA5 and IMERG are equally helpful as APHRODITE to predict the non-exceedance and exceedance probabilities of the dependent variables.

4.1 Assessment of Risk of TWSC for given Precipitation Scenarios

The magnitude of the non-exceedance probability of TWSC (≤ 5th percentile) for different scenarios of ERA5 follows a very similar pattern to that of when obtained for the scenarios of APHRODITE, whereas the conditional distributions of TWSC with respect to IMERG lie between the other two products. It is observed that lower values of TWSC are more sensitive to lower precipitation values for all the precipitation products. In contrast, the sensitivity of TWSC reduces with an increase in precipitation. For instance, when precipitation is less than equal to the 95th percentile, the sensitivity of TWSC reduces by as much as about a third/fourth of when precipitation is less than equal to 5th percentile. This could be because smaller rainfall events have more opportunity for infiltration and get into the groundwater system than for larger storm events, which could flow as runoff to surface water bodies.

The harmonization of low extremes precipitation and TWSC occur during November – January and high extremes during June – September, which is reported elsewhere (Jia et al., 2020). Though the periods of harmonization are different, the present study covers not only the upper part of the Brahmaputra basin but also the whole basin. Moreover, there was a modulation between wetness and dryness of the lower and upper parts of the basin (Chun et al., 2020). The dependence structure of the joint distribution of TWSC-precipitation can evaluate the risk to about the same degree irrespective of precipitation data (Bibi et al., 2019). This is helpful, particularly for Brahmaputra basin, which is poorly gauged due to inhospitable terrain and has varying topographic features and climate making it too difficult to record in-situ hydrometeorological data.

4.2 Assessment of Risk of ET for given Precipitation Scenarios

ET is the link between water and energy budgets. Hence, it is necessary to understand its role in water budget and cycle components assessment. ET estimation could be useful to determine the water availability of the basin (Li et al., 2019). The non-exceedance probability of ET beyond 25th percentile of ERA5 is similar to that with the other two precipitation data. This behavior of lower probabilities of occurrence of ET may be attributed to the higher precipitation amount of ERA5 for lower percentiles (≤5th, 25th) because it is seen that with the increase in the precipitation, the probabilities of ET decrease. Lower precipitation events have higher chances of evaporating than higher ones. It is evident from the values of APHRODITE and IMERG precipitation (Figure 8 (a), (b)) at ≤ 5th percentile, which is about 1/8 of ERA5 as shown in Table 5. It is more than 1/3 of ERA5 for APHRODITE and IMERG precipitation ≤ 25th percentile. It is noteworthy that beyond 25th percentile of precipitation, ERA5 precipitation is a little more than one time of the other two precipitation products. The exceedance probabilities of ET increase with increase in precipitation. Such probabilities are negligible during non-monsoon season because it is very much less likely for a small amount of rainfall to contribute to a large amount of ET.

4.3 Assessment of Risk of Q for given Precipitation Scenarios

It is to be noted that the probabilities of occurrence of Q for APHRODITE and IMERG are very similar in pattern to each other, probably since IMERG is gauge-corrected satellite precipitation leading to a closer estimate of precipitation. However, the probabilities of occurrence of Q given ERA5 are different for scenarios up to ≤5th, 25th compared to given APHRODITE and IMERG. Though the magnitude of ERA5 ≤ 5th percentile is about eight times (Table 5) to that of APHRODITE and IMERG (≤5th percentile), the probability of occurrence of Q (≤5th percentile) given ERA5 is only about one half when compared to given APHRODITE and IMERG in this scenario. The non-exceedance predictive capability of APHRODITE and IMERG for discharge is very similar as both the products are linked to in-situ measurements.

Though APHRODITE and IMERG are better at predicting low flows, all three products equally perform to predict high flows. The non-exceedance probabilities of Q decrease with the increase in precipitation by almost three times (from 5th to 95th percentile). In contrast, the exceedance probabilities increase with increase in precipitation by about two times. This is because higher precipitation has a greater likelihood of causing a flood or a high flow. It is well known that the Brahmaputra basin experiences flood every year when maximum precipitation occurs during monsoon season, leading to a high flow level in the river. Hence, the copula concept in this context could be used for water supply management and flood control (Liu et al., 2016; Liu and Menzel, 2018). Copula could also be helpful to determine the threshold of low flow for the ecological balance of the Brahmaputra river.

The limitation of bivariate copula is that if a variable is controlled by more than one variable, the probabilistic prediction may not be a representative of the actual prediction (Bibi et al., 2019). However, as a preliminary study, the present research could be extended to more than two variables. To further explore this investigation, it is recommended to use hierarchical/ vine copulas to model the dependence structure of more than two variables. Also, the interaction between ET-Q, ET - TWSC, and TWSC-Q pairs could be explored. In addition to these combinations, TWSC was not subdivided into different components like snow water equivalent storage (SWE), groundwater storage (GWS), and soil moisture storage (SMS). Future studies could look into the probabilistic prediction of the sub components of TWSC for the same scenarios of a given precipitation used in this study by extending the work of (Shamsudduha and Taylor, 2020). Probabilistic predictions could also be carried out on a seasonal basis (Bibi et al., 2019).

5. Conclusion

Precipitation is known to be the major component of the terrestrial water cycle. Precipitation data obtained from gauge records is plagued by wind-induced under-catch and altitude bias. It is also sparsely recorded in mountainous regions. Reanalysis data are derived from model and are not gauge corrected. Satellite-based precipitation has wide coverage but can under/over predict low/high precipitation depending on the climate of a region. For a transboundary basin like Brahmaputra where gauge data of hydrometeorological variables are rarely available in the public domain, the alternative is to use the data sets obtained from various types as stated above.

This study is the first attempt to conduct a comparative study of APHRODITE, ERA5, and IMERG to probabilistically predict TWSC, ET, and Q for a large river basin, the Brahmaputra using the concept of dependence structure and copulas. In this study, a bivariate dependence structure was constructed to predict the conditional distributions of TWSC, ET, and Q for different precipitation scenarios. Based on the KS-statistic and p-values, the optimal marginal distributions are gamma for APHRODITE and IMERG, lognormal for ERA5 and discharge, normal kernel density function for TWSC, and logistic for ET. The optimal copulas are Frank for all the three precipitation-TWSC pairs, ERA5-ET, and ERA5-Q, Clayton for the remaining pairs. The Pearson's linear and Spearman's rank correlations for all the pairs of variables are significant for observed and simulated values. The non-exceedance probability of all the dependent variables (lower percentile) decreases with an increase in precipitation. However, the exceedance probability of the same variables (upper percentile) increases gradually with an increase in precipitation.

References

Abudu, S., King, J.P., Pagano, T.C., 2010. Application of Partial Least-Squares Regression in Seasonal Streamflow Forecasting. J. Hydrol. Eng., 15, Pp. 612–623. https://doi.org/10.1061/(ASCE)HE.1943-5584.0000216

AghaKouchak, A., Mehran, A., 2013. Extended contingency table: Performance metrics for satellite observations and climate model simulations. Water Resour. Res., 49, Pp. 7144–7149. https://doi.org/10.1002/wrcr.20498

Ahmad, N., Lodrick, D.O., 2017. Brahmaputra River [WWW Document]. Br. Online Encycl. URL https://www.britannica.com/place/Brahmaputra-River (accessed 5.15.17).

Ahn, K.H., Palmer, R.N., 2016. Use of a nonstationary copula to predict future bivariate low flow frequency in the Connecticut river basin. Hydrol. Process., 30, Pp. 3518–3532. https://doi.org/10.1002/hyp.10876

Almanaseer, N., Sankarasubramanian, A., 2012. Role of Climate Variability in Modulating the Surface Water and Groundwater Interaction over the Southeast United States. J. Hydrol. Eng. 17, Pp. 1001–1010. https://doi.org/10.1061/(ASCE)HE.1943-5584.0000536

Bibi, S., Wang, L., Li, X., Zhang, X., Chen, D., 2019. Response of Groundwater Storage and Recharge in the Qaidam Basin (Tibetan Plateau) to Climate Variations From 2002 to 2016. J. Geophys. Res. Atmos., 124, Pp. 9918–9934. https://doi.org/10.1029/2019JD030411

Chun, K.P., He, Q., Fok, H.S., Ghosh, S., Yetemen, O., Chen, Q., Mijic, A., 2020. Gravimetry-based water storage shifting over the China-India border area controlled by regional climate variability. Sci. Total Environ., 714, Pp. 136360. https://doi.org/10.1016/j.scitotenv.2019.136360

Duan, Z., Liu, J., Tuo, Y., Chiogna, G., Disse, M., 2016. Evaluation of eight high spatial resolution gridded precipitation products in Adige Basin (Italy) at multiple temporal and spatial scales. Sci. Total Environ., 573, Pp. 1536–1553. https://doi.org/10.1016/j.scitotenv.2016.08.213

Futter, M.N., Whitehead, P.G., Sarkar, S., Rodda, H., Crossman, J., 2015. Rainfall runoff modelling of the Upper Ganga and Brahmaputra basins using PERSiST. Environ. Sci. Process. Impacts., 17, Pp. 1070–1081. https://doi.org/10.1039/C4EM00613E

Genest, C., Favre, A.C., 2007. Everything You Always Wanted to Know about Copula Modeling but Were Afraid to Ask. J. Hydrol. Eng., 12, Pp. 347–368. https://doi.org/10.1061/(ASCE)1084-0699(2007)12:4(347)

Han, X., Wei, Z., Zhang, B., Li, Y., Du, T., Chen, H., 2021. Crop evapotranspiration prediction by considering dynamic change of crop coefficient and the precipitation effect in back-propagation neural network model. J. Hydrol., 596, Pp. 126104. https://doi.org/10.1016/j.jhydrol.2021.126104

Hao, Z., Hao, F., Singh, V.P., Sun, A.Y., Xia, Y., 2016. Probabilistic prediction of hydrologic drought using a conditional probability approach based on the meta-Gaussian model. J. Hydrol., 542, Pp. 772–780. https://doi.org/10.1016/j.jhydrol.2016.09.048

Hao, Z., Hao, F., Singh, V.P., Xia, Y., Shi, C., Zhang, X., 2018. A multivariate approach for statistical assessments of compound extremes. J. Hydrol., 565, Pp. 87–94. https://doi.org/10.1016/j.jhydrol.2018.08.025

Hasan, E., Tarhule, A., 2020. GRACE: Gravity Recovery and Climate Experiment long-term trend investigation over the Nile River Basin: Spatial variability drivers. J. Hydrol., 586, Pp. 124870. https://doi.org/10.1016/j.jhydrol.2020.124870

Hasson, S., Lucarini, V., Pascale, S., 2013. Hydrological cycle over South and Southeast Asian River basins as simulated by PCMDI/CMIP3 experiments. Earth Syst. Dyn. 4, Pp. 199–217. https://doi.org/10.5194/esd-4-199-2013

Hersbach, H., Bell, B., Berrisford, P., Hirahara, S., Horányi, A., Muñoz-Sabater, J., Nicolas, J., Peubey, C., Radu, R., Schepers, D., Simmons, A., Soci, C., Abdalla, S., Abellan, X., Balsamo, G., Bechtold, P., Biavati, G., Bidlot, J., Bonavita, M., Chiara, G., Dahlgren, P., Dee, D., Diamantakis, M., Dragani, R., Flemming, J., Forbes, R., Fuentes, M., Geer, A., Haimberger, L., Healy, S., Hogan, R.J., Hólm, E., Janisková, M., Keeley, S., Laloyaux, P., Lopez, P., Lupu, C., Radnoti, G., Rosnay, P., Rozum, I., Vamborg, F., Villaume, S., Thépaut, J., 2020. The ERA5 global reanalysis. Q. J. R. Meteorol. Soc. 146, Pp. 1999–2049. https://doi.org/10.1002/qj.3803

Hu, Z., Zhang, Z., Sang, Y.F., Qian, J., Feng, W., Chen, X., Zhou, Q., 2021. Temporal and spatial variations in the terrestrial water storage across Central Asia based on multiple satellite datasets and global hydrological models. J. Hydrol., 596, Pp. 126013. https://doi.org/10.1016/j.jhydrol.2021.126013

Huffman, G.J., Stocker, E.F., Bolvin, D.T., Nelkin, E.J., Tan, J., 2019. GPM IMERG Final Precipitation L3 1 day 0.1-degree x 0.1-degree V06, Edited by Andrey Savtchenko, Greenbelt, MD, Goddard Earth Sciences Data and Information Services Center (GES DISC) [WWW Document]. https://doi.org/https://doi.org/10.5067/GPM/IMERGDF/DAY/06

Immerzeel, W., 2008. Historical trends and future predictions of climate variability in the Brahmaputra basin. Int. J. Climatol., 28, Pp. 243–254. https://doi.org/10.1002/joc.1528

Jato-Espino, D., Charlesworth, S.M., Perales-Momparler, S., Andrés-Doménech, I., 2017. Prediction of Evapotranspiration in a Mediterranean Region Using Basic Meteorological Variables. J. Hydrol. Eng., 22, Pp. 04016064. https://doi.org/10.1061/(ASCE)HE.1943-5584.0001485

Ji, X., Li, Y., Luo, X., He, D., Guo, R., Wang, J., Bai, Y., Yue, C., Liu, C., 2020. Evaluation of bias correction methods for APHRODITE data to improve hydrologic simulation in a large Himalayan basin. Atmos. Res., 242, Pp. 104964. https://doi.org/10.1016/j.atmosres.2020.104964

Jia, Y., Lei, H., Yang, H., Hu, Q., 2020. Terrestrial Water Storage Change Retrieved by GRACE and Its Implication in the Tibetan Plateau: Estimating Areal Precipitation in Ungauged Region. Remote Sens., 12, Pp. 3129. https://doi.org/10.3390/rs12193129

Jian, J., Webster, P.J., Hoyos, C.D., 2009. Large-scale controls on Ganges and Brahmaputra River discharge on intrapersonal and seasonal timescales. Q. J. R. Meteorol. Soc., 135, Pp. 353–370. https://doi.org/10.1002/qj.384

Legates, D.R., McCabe, G.J., 1999. Evaluating the use of "goodness-of-fit" Measures in hydrologic and hydroclimatic model validation. Water Resour. Res., 35, Pp. 233–241. https://doi.org/10.1029/1998WR900018

Li, C., Sun, G., Caldwell, P. V., Cohen, E., Fang, Y., Zhang, Y., Oudin, L., Sanchez, G.M., Meentemeyer, R.K., 2020. Impacts of Urbanization on Watershed Water Balances Across the Conterminous United States. Water Resour. Res., 56. https://doi.org/10.1029/2019WR026574

Li, J.Z., Wang, Y.X., Li, S.F., Hu, R., 2015. A Nonstationary Standardized Precipitation Index incorporating climate indices as covariates. J. Geophys. Res. Atmos., 120, Pp. 12,082-12,095. https://doi.org/10.1002/2015JD023920

Li, X., Long, D., Han, Z., Scanlon, B.R., Sun, Z., Han, P., Hou, A., 2019. Evapotranspiration Estimation for Tibetan Plateau Headwaters Using Conjoint Terrestrial and Atmospheric Water Balances and Multisource Remote Sensing. Water Resour. Res., 55, Pp. 8608–8630. https://doi.org/10.1029/2019WR025196

Li, Z., Quiring, S.M., 2021. Investigating spatial heterogeneity of the controls of surface water balance in the contiguous United States by considering anthropogenic factors. J. Hydrol., 601, Pp. 126621. https://doi.org/10.1016/j.jhydrol.2021.126621

Li, Z., Tang, G., Hong, Z., Chen, M., Gao, S., Kirstetter, P., Gourley, J.J., Wen, Y., Yami, T., Nabih, S., Hong, Y., 2021. Two-decades of GPM IMERG early and final run products intercomparison: Similarity and difference in climatology, rates, and extremes. J. Hydrol. 594, Pp. 125975. https://doi.org/10.1016/j.jhydrol.2021.125975

Liu, Z., Chen, X., Liu, F., Lin, K., He, Y., Cai, H., 2018. Joint Dependence Between River Water Temperature, Air Temperature, and Discharge in the Yangtze River: The Role of the Three Gorges Dam. J. Geophys. Res. Atmos., 123, 11, Pp. 938-11,951. https://doi.org/10.1029/2018JD029078

Liu, Z., Menzel, L., 2018. Probabilistic dependence between streamflow and hydroclimatic variables and the possible linkages to large-scale atmospheric circulation: A case study in Baden-Württemberg, Southwest Germany. J. Hydrol., 565, Pp. 443–454. https://doi.org/10.1016/j.jhydrol.2018.08.054

Liu, Z., Törnros, T., Menzel, L., 2016. A probabilistic prediction network for hydrological drought identification and environmental flow assessment. Water Resour. Res., 52, Pp. 6243–6262. https://doi.org/10.1002/2016WR019106

Masood, M., Yeh, P.J.F., Hanasaki, N., Takeuchi, K., 2015. Model study of the impacts of future climate change on the hydrology of Ganges–Brahmaputra–Meghna basin. Hydrol. Earth Syst. Sci., 19, Pp. 747–770. https://doi.org/10.5194/hess-19-747-2015

McCabe, M.F., Rodell, M., Alsdorf, D.E., Miralles, D.G., Uijlenhoet, R., Wagner, W., Lucieer, A., Houborg, R., Verhoest, N.E.C., Franz, T.E., Shi, J., Gao, H., Wood, E.F., 2017. The future of Earth observation in hydrology. Hydrol. Earth Syst. Sci., 21, Pp. 3879–3914. https://doi.org/10.5194/hess-21-3879-2017

Mu, Q., Zhao, M., Running, S.W., 2011. Improvements to a MODIS global terrestrial evapotranspiration algorithm. Remote Sens. Environ., 115, Pp. 1781–1800. https://doi.org/10.1016/j.rse.2011.02.019

Muthuvel, D., Mahesha, A., 2021. Copula-Based Frequency and Coincidence Risk Analysis of Floods in Tropical-Seasonal Rivers. J. Hydrol. Eng., 26, Pp. 05021007. https://doi.org/10.1061/(ASCE)HE.1943-5584.0002061

Ndehedehe, C., Awange, J., Agutu, N., Kuhn, M., Heck, B., 2016. Understanding changes in terrestrial water storage over West Africa between 2002 and 2014. Adv. Water Resour., 88, Pp. 211–230. https://doi.org/10.1016/j.advwatres.2015.12.009

Nelsen, R.B., 2006. An Introduction to Copulas, Springer Series in Statistics.

Springer New York, New York, NY. https://doi.org/10.1007/0-387-28678-0

Nogueira, M., 2020. Inter-comparison of ERA-5, ERA-interim and GPCP rainfall over the last 40 years: Process-based analysis of systematic and random differences. J. Hydrol., 583, Pp. 124632. https://doi.org/10.1016/j.jhydrol.2020.124632

Oliveira, P.T.S., Wendland, E., Nearing, M.A., Scott, R.L., Rosolem, R., da Rocha, H.R., 2015. The water balance components of undisturbed tropical woodlands in the Brazilian cerrado. Hydrol. Earth Syst. Sci., 19, Pp. 2899–2910. https://doi.org/10.5194/hess-19-2899-2015

Pellet, V., Aires, F., Papa, F., Munier, S., Decharme, B., 2020. Long-term total water storage change from a Satellite Water Cycle reconstruction over large southern Asian basins. Hydrol. Earth Syst. Sci., 24, Pp. 3033–3055. https://doi.org/10.5194/hess-24-3033-2020

Pervez, M.S., Henebry, G.M., 2015. Assessing the impacts of climate and land use and land cover change on the freshwater availability in the Brahmaputra River basin. J. Hydrol. Reg. Stud., 3, Pp. 285–311. https://doi.org/10.1016/j.ejrh.2014.09.003

Poncelet, C., Merz, R., Merz, B., Parajka, J., Oudin, L., Andréassian, V., Perrin, C., 2017. Process-based interpretation of conceptual hydrological model performance using a multinational catchment set. Water Resour. Res., 53, Pp. 7247–7268. https://doi.org/10.1002/2016WR019991

Sahana, V., Timbadiya, P.V., 2020. Spatiotemporal Variation of Water Availability under Changing Climate: Case Study of the Upper Girna Basin, India. J. Hydrol. Eng., 25, Pp. 05020004. https://doi.org/10.1061/(ASCE)HE.1943-5584.0001890

Sajeev, A., Deb Barma, S., Mahesha, A., Shiau, J.T., 2021. Bivariate Drought Characterization of Two Contrasting Climatic Regions in India Using Copula. J. Irrig. Drain. Eng., 147, Pp. 05020005. https://doi.org/10.1061/(ASCE)IR.1943-4774.0001536

Salvadori, G., De Michele, C., 2004. Frequency analysis via copulas: Theoretical aspects and applications to hydrological events. Water Resour. Res., 40. https://doi.org/10.1029/2004WR003133

Seyoum, W.M., Kwon, D., 2020. Suitability of satellite-based hydro-climate variables and machine learning for streamflow modeling at various scale watersheds. Hydrol. Sci. J., 65, Pp. 2233–2248. https://doi.org/10.1080/02626667.2020.1792473

Shamsudduha, M., Taylor, R.G., 2020. Groundwater storage dynamics in the world's large aquifer systems from GRACE: uncertainty and role of extreme precipitation. Earth Syst. Dyn., 11, Pp. 755–774. https://doi.org/10.5194/esd-11-755-2020

Sharannya, T.M., Al-Ansari, N., Barma, S.D., Mahesha, A., 2020. Evaluation of Satellite Precipitation Products in Simulating Streamflow in a Humid Tropical Catchment of India Using a Semi-Distributed Hydrological Model. Water 2020, Vol. 12, Page 2400 12, 2400. https://doi.org/10.3390/W12092400

Sheffield, J., Wood, E.F., Pan, M., Beck, H., Coccia, G., Serrat-Capdevila, A., Verbist, K., 2018. Satellite Remote Sensing for Water Resources Management: Potential for Supporting Sustainable Development in Data-Poor Regions. Water Resour. Res., 54, Pp. 9724–9758. https://doi.org/10.1029/2017WR022437

Sheikholeslami, R., Gharari, S., Papalexiou, S.M., Clark, M.P., 2021. VISCOUS: A Variance-Based Sensitivity Analysis Using Copulas for Efficient Identification of Dominant Hydrological Processes. Water Resour. Res., 57. https://doi.org/10.1029/2020WR028435

Shiau, J.T., Lien, Y.C., 2021. Copula-Based Infilling Methods for Daily Suspended Sediment Loads. Water, 13, Pp. 1701. https://doi.org/10.3390/w13121701

Shojaeezadeh, S.A., Nikoo, M.R., McNamara, J.P., AghaKouchak, A., Sadegh, M., 2018. Stochastic modeling of suspended sediment load in alluvial rivers. Adv. Water Resour. 119, Pp. 188–196. https://doi.org/10.1016/j.advwatres.2018.06.006

Sinha, J., Jha, S., Goyal, M.K., 2019. Influences of watershed characteristics on long-term annual and intra-annual water balances over India. J. Hydrol., 577, Pp. 123970. https://doi.org/10.1016/j.jhydrol.2019.123970

Sridhar, V., Ali, S.A., Lakshmi, V., 2019. Assessment and validation of total water storage in the Chesapeake Bay watershed using GRACE. J. Hydrol. Reg. Stud., 24, Pp. 100607. https://doi.org/10.1016/j.ejrh.2019.100607

Sun, A.Y., Wang, D., Xu, X., 2014. Monthly streamflow forecasting using Gaussian Process Regression. J. Hydrol., 511, Pp. 72–81. https://doi.org/10.1016/j.jhydrol.2014.01.023

Tao, Y., Wang, Y., Wang, D., Ni, L., Wu, J., 2020. A probabilistic modeling framework for assessing the impacts of large reservoirs on river thermal regimes – A case of the Yangtze River. Environ. Res., 183, Pp. 109221. https://doi.org/10.1016/j.envres.2020.109221

Tapley, B.D., Bettadpur, S., Ries, J.C., Thompson, P.F., Watkins, M.M., 2004. GRACE Measurements of Mass Variability in the Earth System. Science (80-). 305, Pp. 503–505. https://doi.org/10.1126/science.1099192

Tavakol, A., Rahmani, V., Harrington Jr., J., 2020. Probability of compound climate extremes in a changing climate: A copula-based study of hot, dry, and windy events in the central United States. Environ. Res. Lett., 15, Pp. 104058. https://doi.org/10.1088/1748-9326/abb1ef

Uttarwar, S.B., Deb Barma, S., Mahesha, A., 2020. Bivariate Modeling of Hydroclimatic Variables in Humid Tropical Coastal Region Using Archimedean Copulas. J. Hydrol. Eng. 25, Pp. 05020026. https://doi.org/10.1061/(ASCE)HE.1943-5584.0001981

Wable, P.S., Jha, M.K., 2018. Application of Archimedean copulas to the impact assessment of hydro-climatic variables in semi-arid aquifers of western India. Hydrogeol. J., 26, Pp. 89–108. https://doi.org/10.1007/s10040-017-1636-7

Wang, S., Huang, J., Li, J., Rivera, A., McKenney, D.W., Sheffield, J., 2014. Assessment of water budget for sixteen large drainage basins in Canada. J. Hydrol., 512, Pp. 1–15. https://doi.org/10.1016/j.jhydrol.2014.02.058

Watkins, M.M., Wiese, D.N., Yuan, D.N., Boening, C., Landerer, F.W., 2015. Improved methods for observing Earth's time variable mass distribution with GRACE using spherical cap mascons. J. Geophys. Res. Solid Earth, 120, Pp. 2648–2671. https://doi.org/10.1002/2014JB011547

Wehbe, Y., Temimi, M., Ghebreyesus, D.T., Milewski, A., Norouzi, H., Ibrahim, E., 2018. Consistency of precipitation products over the Arabian Peninsula and interactions with soil moisture and water storage. Hydrol. Sci. J., 63, Pp. 408–425. https://doi.org/10.1080/02626667.2018.1431647

Yatagai, A., Kamiguchi, K., Arakawa, O., Hamada, A., Yasutomi, N., Kitoh, A., 2012. APHRODITE: Constructing a Long-Term Daily Gridded Precipitation Dataset for Asia Based on a Dense Network of Rain Gauges. Bull. Am. Meteorol. Soc., 93, Pp. 1401–1415. https://doi.org/10.1175/BAMS-D-11-00122.1

Yuan, R.Q., Chang, L.L., Gupta, H., Niu, G.Y., 2019. Climatic forcing for recent significant terrestrial drying and wetting. Adv. Water Resour., 133, Pp. 103425. https://doi.org/10.1016/j.advwatres.2019.103425

Zhang, L., Singh, V.P., 2006. Bivariate Flood Frequency Analysis Using the Copula Method. J. Hydrol. Eng., 11, Pp. 150–164. https://doi.org/10.1061/(ASCE)1084-0699(2006)11:2 (150)

Zhou, W., Guan, K., Peng, B., Shi, J., Jiang, C., Wardlow, B., Pan, M., Kimball, J.S., Franz, T.E., Gentine, P., He, M., Zhang, J., 2020. Connections between the hydrological cycle and crop yield in the rainfed U.S. Corn Belt. J. Hydrol., 590, Pp. 125398. https://doi.org/10.1016/j.jhydrol.2020.125398

Zscheischler, J., Seneviratne, S.I., 2017. Dependence of drivers affects risks associated with compound events. Sci. Adv. 3, Pp. e1700263. https://doi.org/10.1126/sciadv.1700263